A Frequency-Dependence Model for the Ultra-Wideband Channel based on Propagation Events

Camillo Gentile and Alfred Kik
National Institute of Standards and Technology
Wireless Communication Technologies Group
Gaithersburg, Maryland, USA

***Abstract*— While the frequency-dependence of the wireless channel may be negligible for narrow to wideband signals, it has been shown that modeling this dependence for bandwidths in excess of 2 GHz improves channel reconstruction up to 40%. Yet to our knowledge, only Molisch et al. have done so for the ultra-wideband channel. Their benchmark frequency model however represents the average dependence over the collection of multi-path arrivals in the channel rather than that of individual arrivals. Building on the Geometric Theory of Diffraction, we propose a novel frequency model for *individual* arrivals according to the propagation events on their paths between the transmitter and receiver. We extract the model parameters from an extensive measurement campaign of 3000 channel frequency sweeps in three separate buildings combined with raytracing simulations, and show that ours fits the gathered data more closely than the benchmark model.**

***Index Terms*— Geometric Theory of Diffraction, GTD**

I. Introduction

Ultra wideband (UWB) signals are characterized by a bandwidth greater than 500 MHz or one exceeding 20% of the center frequency of radiation [1], [2]. The approval of the FCC unlicensed band from 3.1-10.6 GHz in 2002 has prompted a concerted effort in the extensive modeling of the indoor UWB channel in recent years. Irahhauten provides a comprehensive overview of indoor UWB measurements in the time and frequency domains [3]. Table I summarizes this overview, but augmented to include reported measurements to date. Most references in the table provide channel models characterized by path loss, small-scale fading, and delay spread.

While the frequency-dependence of the wireless channel may be negligible for narrow to wideband signals, it has been shown that modeling this dependence for bandwidths in excess of 2 GHz improves channel reconstruction up to 40% [12]. Yet to our knowledge, only Molisch et al. have done so for the ultra-wideband channel. Their benchmark frequency model however represents the average dependence over the collection of multi-path arrivals in the channel rather than that of individual arrivals. This paper proposes a novel frequency model for *individual* arrivals.

The paper reads as follows: similar to [8], [9], [10], [11], Section II outlines our channel measurement campaign consisting of a total of 3000 frequency sweeps from 2-6.5 GHz in three separate buildings. The Geometric Theory of Diffraction (GTD) provides a basis for the frequency-dependence of individual arrivals according to the propagation events on their paths between the transmitter and receiver. Building on this theory, the first contribution of this paper is the GTD-based frequency model in Section III whose parameters are characterized from the measurement campaign. While significantly more accurate than the benchmark model, it accounts only for the geometry of the buildings and not the material properties of the walls. Section IV features our main contribution as an extension of the GTD-based model incorporating the material properties as well. The proposed model fits the gathered data more closely than both the benchmark and the GTD-based models as highlighted in the results section V, following by our conclusions.

	Prin. Investigator	f range	environment	range
time	Yano [4]	1.25-2.75 GHz	office	17 m
	Cassioli [2], [6], [7]	3.6-6 GHz	office	18 m
	Prettie [5]	2-8 GHz	res.	20 m
frequency	Kunisch [8]	1-11 GHz	office	10 m
	Keignart [9]	2-6 GHz	office / res.	20 m
	Ghassemzadeh [10]	2-8 GHz	res. / commercial	15 m
	Molisch [11]	3-10 GHz	res. / industrial / office	28 m 20 m

TABLE I
Overview of reported indoor UWB measurements.

II. Preliminaries

A. The frequency-dependent indoor channel

The frequency-dependent indoor channel consists of an impulse train representing K multi-path arrivals indexed through k [12]

$$H(f) = \sum_{k=1}^{K} a_k \left(\frac{f}{f_0}\right)^{-\alpha_k} e^{-j2\pi f \tau_k}, \qquad (1)$$

where τ_k denotes the delay of the arrival in propagating between the transmitter and receiver and a_k denotes the complex-valued amplitude which accounts for both attenuation and phase shift due to transmission, reflection, and diffraction introduced by walls (and other objects) on its path. The *frequency parameter* α_k quantifies the frequency-dependence of the amplitude across the bandwidth of the signal, where f_0 is the lower frequency. The frequency-dependent indoor channel has been shown to improve reconstruction up to 40% for bandwidths in excess of 2 GHz [12] compared to the conventional which assumes $\alpha_k = 0$ [13].

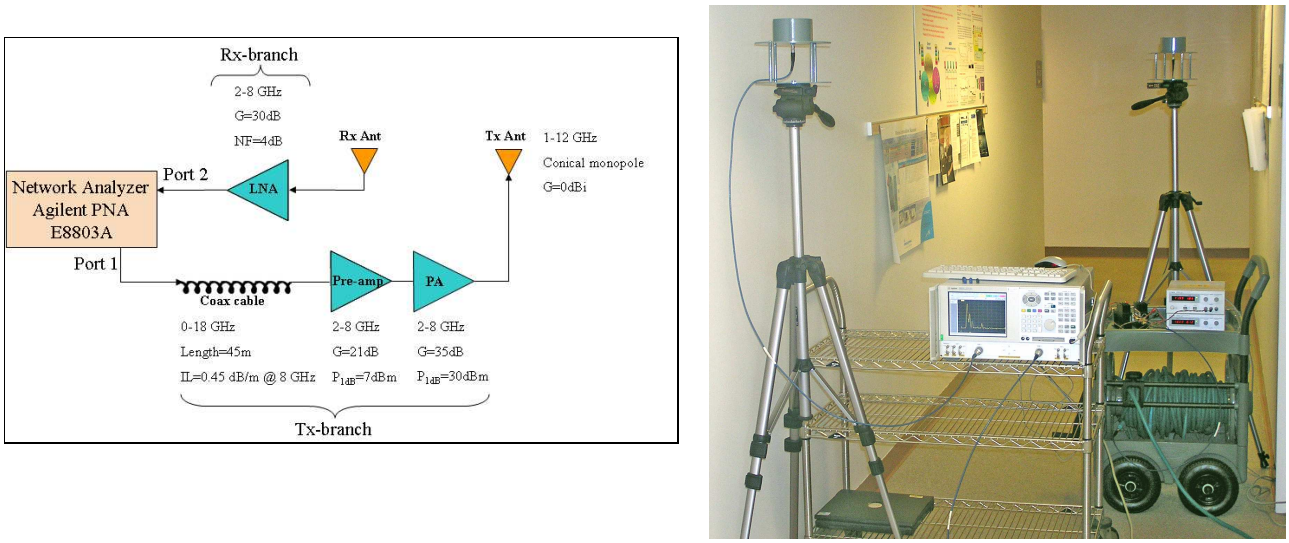

(a) Block diagram

(b) Photograph

Fig. 1. The measurement system using the Vector Network Analyzer.

B. The measurement system

We measured the frequency response of the channel $H(f)$ with sampling interval Δf in the bandwidth f = 2 – 6.5 GHz; a discrete frequency spectrum translates to a periodic signal in the time domain with period $\frac{1}{\Delta f}$ [14]. Choosing Δf = 1.25 MHz allows for a maximum multipath spread of 800 ns, which proves sufficient throughout all three buildings for the arrivals to subside and avoid time aliasing.

Fig. 1 displays the block diagram and photograph of our measurement system. The vector network analyzer (VNA) emits a series of tones with frequency f at Port 1 and measures the relative amplitude and phase $S_{21}(f)$ at Port 2, providing automatic phase synchronization between the two ports. The synchronization translates to a common time reference for the transmitted and received signals. The long cable enables variable positioning of the conical monopole antennas from each other throughout the test area. The preamplifier and power amplifier on the transmit branch boost the signal such that it radiates at approximately 30 dBm from the antenna. After it passes through the channel, the low-noise amplifier (LNA) on the receiver branch boosts the signal above the noise floor of Port 2 before feeding it back.

The $S_{21}(f)$-parameter of the network in Fig. 1 can be expressed as a product of the Tx-branch, the Tx-antenna, the propagation channel, the Rx-antenna, and the Rx-branch

$$\begin{aligned} S_{21}(f) &= H_{Tx}^{bra}(f) \cdot H_{Tx}^{ant}(f) \cdot H(f) \cdot H_{Rx}^{ant}(f) \cdot H_{Rx}^{bra}(f) \\ &= H_{Tx}^{bra}(f) \cdot \underbrace{H_{Tx}^{ant}(f) \cdot H_{Rx}^{ant}(f)}_{H^{ant}(f)} \cdot H(f) \cdot H_{Rx}^{bra}(f). \end{aligned}$$

The frequency response of the channel H is extracted by individually measuring the transmission responses $H_{Tx}^{bra}, H_{Rx}^{bra}$, and H^{ant} in advance and de-embedding them from (2). Measuring the characteristics of the antennas on a flat open field with dimensions exceeding 100 m $\times$ 100 m reduced ambient multi-path to a single ground bounce which we removed by placing electromagnetic absorbers on the ground between the antennas. We separated the antennas by a distance of 1.5 m to avoid the near-field effects and spatially averaging them through rotation with respect to each other every ten degrees [15]. Their height was set to 1.7 m (average human height).

Note in particular the following implementation considerations:

- to account for the frequency-dependent loss in the long cable when operating across such a large bandwidth, we ramped up the emitted power at Port 1 with increasing frequency to radiate from the antenna at approximately 30 dBm across the whole band;
- we removed the LNA from the network in experiments with range below 10 m to protect it from overload and also avert its operation in the non-linear region;
- to extend the dynamic range of our system, we exploited the configurable test set option of the VNA to reverse the signal path in the coupler of Port 2 and bypass the 12 dB loss associated with the coupler arm. The dynamic range of the propagation channel corresponds to 140 dB as computed through [9] for an IF bandwidth of 1 kHz and a SNR of 15 dB at the receiver;
- to account for the small-scale effects in the measurements, for each experiment we centered a 5×5 grid constructed from a wooden plank on the floor about the nominal location of the receiver antenna. The distance between the grid points was 15 cm, corresponding to a full wavelength at 2 GHz, ensuring spatial independence between the measured points for a total of 25 sub-experiments.

TABLE II

EXPERIMENTS CONDUCTED IN MEASUREMENT CAMPAIGN.

building	wall material	LOS range (10)	NLOS range (30)
NIST North	sheet rock / aluminum studs	1.2-24.3 m	1.7-30.5 m max wall#: 9
Child Care	plaster / wooden studs	2.0-15.7 m	4.7-26.7 m max wall#: 6
Sound	cinder block	3.4-45.0 m	5.9-28.9 m max wall#: 6

TABLE III

THE GTD-BASED COMPONENTS OF THE FREQUENCY PARAMETER.

propagation events	α^E
free space	0.0
transmission	0.0
reflection	0.0
edge diffraction	0.5
corner diffration	1.0
cylinder face diffraction	-0.5
cylinder broadside diffraction	-1.0

C. The measurement campaign

The measurement campaign was conducted in three separate buildings on the NIST campus in Gaitherburg, Maryland, each constructed from a dominant wall material varying from sheet rock to cinder block. Table IV summarizes the 40 experiments in each building (10 line-of-sight (LOS) and 30 non line-of-sight (NLOS)), including the maximum number of walls separating the transmitter and receiver.

Spectral estimation methods exist to decompose the measured frequency response of a sub-experiment into K arrivals parameterized as (a_k, α_k, τ_k) according to (1) [16], [17], [18]. The chosen method becomes increasingly important with the presence of noise in the channel. The *SVD-Prony* [17] and *SVD-Eigenpencil* [18] are two candidate methods robust to high levels of noise. We compared the two in estimating the frequency parameter of the first arrival known as $\alpha_1 = 0$ for free space propagation in the combined 30 LOS experiments from the three buildings. Qiu claims that the *SVD-Eigenpencil* decomposition method works reliably above an SNR of 15 dB which corresponds to 140 dB path loss for our measurement system (see II-B). Hence we filtered out the least significant arrivals with power below the equivalent level of 10^{-7} in linear scale. The averages and standard deviations over the 25×30 sub-experiments yielded μ_{α_1} = 0.0879 and σ_{α_1} = 0.1254 for the *SVD-Prony* method and μ_{α_1} = 0.0345 and σ_{α_1} = 0.0567 for the *SVD-Eigenpencil* method, hence we implemented the latter better suited to our application.

III. THE GTD-BASED FREQUENCY MODEL

The Geometric Theory of Diffraction (GTD) has been used in channel characterization [12], [18] to interpret the frequency-dependence of an individual arrival according to the sequence of propagation events on its path: each interaction classified in Table III adds a component α^E to the aggregate frequency parameter α of the arrival [19]. The three buildings in the measurement campaign are void for the most part of cylindrical objects such as rounded columns or furniture with dimensions comparable to the signal wavelength[1], allowing us to disregard cylindrical face and broadside diffractions as confirmed through the measurement campaign in which we recorded no arrivals with negative frequency parameter. In addition, the cumulative surface area of corners with respect to edges is negligible in modeling the significant characteristics of the environment, allowing us to disregard corner diffractions as well.

Since edge diffraction defaults as the only significant propagation mechanism with nonzero component α^E, knowing the *order* n of an arrival, defined as the number of diffractions on its path, directly maps to the frequency parameter of the arrival as

$$\alpha = 0.5 \cdot n, \tag{2}$$

completing the GTD-based frequency model. The remainder of this section develops a probability distribution for n whose parameters are estimated through the measurement campaign in II-C.

A. Modeling the λ^D-parameter

Consider an arrival which undergoes n diffraction events on its path: once an event occurs with delay τ, the delay of the next event $\tau + \Delta\tau$ depends only on the randomly-located objects throughout the environment rather than on τ, and so the *interevent delays* $\Delta\tau$ are independent of each other. The Poisson process [20] models this behavior and is governed through the probability density function for $\Delta\tau$

$$f(\Delta\tau|\lambda^D) = \lambda^D e^{-\lambda^D \Delta\tau}, \tag{3}$$

where $\frac{1}{\lambda^D}$ represents the average delay between diffractions.

In order to estimate the λ^D-parameter, the arrivals from each sub-experiment in II-C were grouped together for each building into a measured (M) sample set of K_M total arrivals parameterized as (a_k, α_k, τ_k). Given the delay τ_k and the observed order $n_k = \frac{\alpha_k}{0.5}$ from (2) in the sample set, the maximum likelihood estimation [21] for λ^D yields

$$\lambda^D = \sum_{k=1}^{K_M} n_k \Bigg/ \sum_{k=1}^{K_M} \tau_k \ . \tag{4}$$

With λ_D known, the sought probability that n diffractions have occured on a path arriving with delay τ follows from (3) as

$$p_(n|\tau, \lambda^D) = \frac{e^{-\lambda^D \tau}(\lambda^D \tau)^n}{n!}, \tag{5}$$

meaning that the reconstructed arrival order is a Poisson random variable $n' \sim \mathcal{P}(\mu_{n'} = \lambda^D\tau, \sigma_{n'} = \sqrt{\lambda^D \tau})$, and $\alpha' =$

[1]The smallest frequency in the bandwidth translates to a wavelength of 15 cm.

$0.5 \cdot n'$ is the reconstructed frequency parameter. Observing the sample set, the frequency parameter on average increases with arrival delay, a phenomenon consistent with our model. The means that a path with a longer delay will on average have undergone more diffractions on the propagation path.

The weighted mean-squared error

$$e = \frac{1}{K_M} \sum_{k=1}^{K_M} \frac{(\alpha_k - \alpha'_k)^2}{\tau_k} \tag{6}$$

gauges the fit between the GTD-based model and the sample set. The weight $w_k = \frac{1}{\tau_k}$ is proportional to the inverse of the variance $\sigma^2_{\alpha'_k} = (0.5 \cdot \sigma_{n'_k})^2 = (0.5 \cdot \sqrt{\lambda^D \tau_k})^2$ typically used to leverage more reliable points. The values for the λ^D-parameter of the GTD-based model and the associated error e for the three buildings appear in Table IV.

IV. The proposed frequency model

The Geometric Theory of Diffraction was developed to characterize the salient features of metal objects such as corners, edges, and curves from radar scattering [19]. The underlying assumption of infinite conductivity renders the frequency parameter dependent only on the object geometry. The theory breaks down for materials with finite conductivity for which material properties and incident angle of diffraction also influence α [22], compromising the values for α^E in Table III and so potentially weighing in the dependencies of the other two dominant propagation mechanisms of transmission and reflection.

In this section, we extend the GTD-based model to account for both geometry *and* material properties as average effects over the incident angles of the propagation mechanisms. To this end, we replace the constant values of α^E with α-parameters $(\alpha^T, \alpha^R, \alpha^D)$ in the proposed model representing transmission, reflection, and diffraction respectively. It follows that the frequency parameter is modeled as the sum of the components of each interaction on a path as

$$\alpha = \alpha^T \cdot l + \alpha^R \cdot m + \alpha^D \cdot n, \tag{7}$$

where (l, m, n) represents the order of the arrival defined as the numbers of tranmissions, reflections, and diffractions respectively. The remainder of this section develops a probability distribution for (l, m, n) and empirically finds values for the α-parameters through the measurement campaign.

A. Modeling the λ-parameters

Consider an arrival which undergoes l transmissions, m reflections, and n diffractions on its path: as for diffraction in III-A, once a propagation event occurs with delay τ, the delay of the next event $\tau + \Delta\tau$ depends only on the randomly-located objects throughout the environment rather than on τ, and so the interevent delays $\Delta\tau$ are independent of each other. So if $p(n|\tau, \lambda^D)$ in (5) is the probability of n diffractions on a path with delay τ, it follows that

$$p(l+m+n|\tau, \lambda) = \frac{e^{-\lambda\tau}(\lambda\tau)^{l+m+n}}{(l+m+n)!} \tag{8}$$

is the probability of $l + m + n$ total propagation events on a path with delay τ, where $\frac{1}{\lambda}$ represents the average delay between events. Further given that $l+m+n$ events have occured, l, m, n are Binomial random variables [20] with respective probabilities $p^T + p^R + p^D = 1$, and

$$p(l, m, n|l+m+n) = \frac{(l+m+n)!}{l!\ m!\ n!}(p^T)^l (p^R)^m (p^D)^n. \tag{9}$$

Now the probability that exactly l transmissions, m reflections, and n diffractions have occured on a path arriving with delay τ follows below by substituting (8) and (9) into

$$\begin{aligned} & p(l, m, n|\tau, \lambda) \\ &= p(l, m, n|l+m+n) \cdot p(l+m+n|\tau, \lambda) \\ &= \underbrace{\frac{e^{-\lambda^T\tau}(\lambda^T\tau)^l}{l!}}_{p(l|\tau,\lambda^T)} \cdot \underbrace{\frac{e^{-\lambda^R\tau}(\lambda^R\tau)^m}{m!}}_{p(m|\tau,\lambda^R)} \cdot \underbrace{\frac{e^{-\lambda^D\tau}(\lambda^D\tau)^n}{n!}}_{p(n|\tau,\lambda^D)}, \end{aligned} \tag{10}$$

and rearranging such that $\lambda^T = p^T\lambda$, $\lambda^R = p^R\lambda$, and $\lambda^D = p^D\lambda$. Hence with the λ-parameters $(\lambda^T, \lambda^R, \lambda^D)$ known, the reconstructed arrival orders are independent Poisson random variables $l' \sim \mathcal{P}(\mu_{l'} = \lambda^T\tau, \sigma_{l'} = \sqrt{\lambda^T\tau})$, $m' \sim \mathcal{P}(\mu_{m'} = \lambda^R\tau, \sigma_{m'} = \sqrt{\lambda^R\tau})$, and $n' \sim \mathcal{P}(\mu_{n'} = \lambda^D\tau, \sigma_{n'} = \sqrt{\lambda^D\tau})$.

In the GTD-based model only diffraction is frequency dependent, and so the diffraction order n_k of an arrival k can be observed from α_k, making it easy to model λ^D through (4). However in the proposed model the order (l_k, m_k, n_k) cannot be determined from α_k, especially when lacking values for the α-parameters. Rather we use radio-frequency raytracing [23], [24] to estimate the λ-parameters in (10) by simulating the sub-experiments described in II-C. A detailed CAD-model of the building characterizes the propagation environment and each sub-experiment is differentiated by the positioning of a transmitter-receiver pair in the building[2] (see Fig. 2). Even though the raytracing tool only runs at a single frequency as opposed to wideband operation, the interevent delays and in turn the λ-parameters depend only on the geometry of the environment and not on the operation frequency. The operation frequency does however change the dielectric properties of the walls, attenuating the amplitude of the arrivals with each propagation event, and as a result affects the number of arrivals delivered when specifying the receiver threshold power. The raytracing simulations were run at the center frequency 4.25 GHz of the bandwidth for which the dielectric properties of the walls are given in [25]. We set the power threshold equal to 10^{-7} as in the measurement campaign. Other relevent settings are the transmission power of 30 dBm and the omni-directional emission pattern of the antennas as in II-B.

[2]The CAD-models lack office furniture present during the measurement campaign.

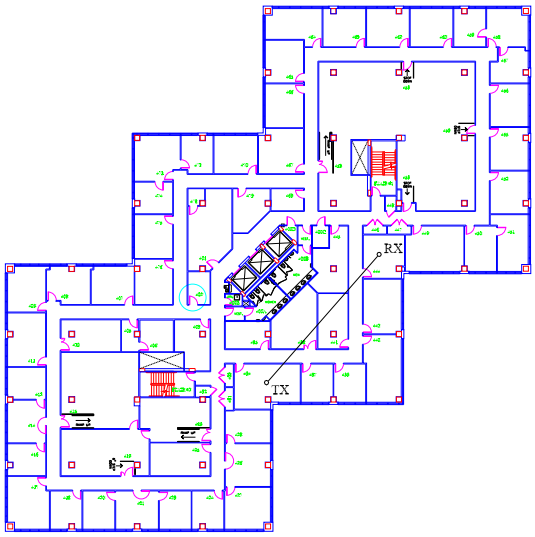

Fig. 2. CAD-model of the *NIST North* building.

The raytracing tool directly generates the impulse response of a sub-experiment described by a train of K arrivals with complex amplitude and delay (a_k, τ_k). Of course knowing the propagation mechanisms on the path, the *WiSE* raytracing software has a feature to furnish the order of the arrival (l_k, m_k, n_k). Parallel to III-A, a simulated (S) sample set of K_S arrivals is gathered from all the sub-experiments in a building from which the maximum likelihood estimation for the λ-parameters yields

$$\begin{aligned} \lambda^T &= \sum_{k=1}^{K_S} l_k \Big/ \sum_{k=1}^{K_S} \tau_k \\ \lambda^R &= \sum_{k=1}^{K_S} m_k \Big/ \sum_{k=1}^{K_S} \tau_k \\ \lambda^D &= \sum_{k=1}^{K_S} n_k \Big/ \sum_{k=1}^{K_S} \tau_k \end{aligned} \quad . \tag{11}$$

B. Modeling the α-parameters

The λ-parameters found above leverage the occurrences of the three propagation mechanisms in (7). Now the same measured sample set of K_M arrivals parameterized as (a_k, α_k, τ_k) used to estimate the λ^D-parameter of the GTD-based model in III-A is used here to estimate rather the α-parameters of the proposed model. The delay τ_k of arrival k maps to the expected reconstructed order $(\mu_{l'_k}, \mu_{m'_k}, \mu_{n'_k})$ through (10) and the expected reconstructed frequency parameter $\alpha'_k = \alpha^T \cdot \mu_{l'_k} + \alpha^R \cdot \mu_{m'_k} + \alpha^D \cdot \mu_{n'_k}$ follows from (7). The values $(\alpha^T, \alpha^R, \alpha^D)$ can be found by minimizing the weighted mean-squared error (see (6)) between the proposed model and the sample set

$$\min_{\alpha^T, \alpha^R, \alpha^D} e = \sum_{k=1}^{K_M} \frac{(\alpha_k - \alpha'_k)^2}{\tau_k}. \tag{12}$$

The values for the λ-parameters and the α-parameters of the proposed model and the associated error e for the three buildings appear in Table IV.

V. Results

A. The benchmark frequency model

This section compares the proposed model to the GTD-based model, and also to the benchmark model in [11]. In the latter, the frequency parameter represents the average dependence over the collection of arrivals rather than that of individual arrivals, hence $\alpha_k = \alpha$ is path-independent. Accordingly the α-parameter is extracted from the measured sample set in III-A using the technique described in [11]. The technique reduces to curve fitting the α-parameter to the amplitude of the measured frequency responses. The weighted mean-squared error for the benchmark model is

$$e = \frac{1}{K_M} \sum_{k=1}^{K_M} \frac{(\alpha_k - \alpha)^2}{\tau_k}, \tag{13}$$

and the values for the α-parameter and the associated error e for the three buildings appear in Table IV.

The benchmark model discriminates between LOS and NLOS conditions in computing separate α^{LOS} and α^{NLOS} for each of the three buildings. In LOS conditions, the signal strength of the first arrival is generally much stronger than the subsequent in the multi-path profile, and so its corresponding frequency parameter $\alpha_1 = 0$ contributes significantly more than the others to α, hence biasing α^{LOS} closer to 0 compared to α^{NLOS}. Rather the path-dependent GTD-based and proposed models can discriminate between the two conditions precisely by explicitly setting the respective probabilities to

$$p(n{=}0|\tau_k, \lambda^D) = \{\ 1, \quad \text{LOS}, k = 1 \tag{14}$$

$$p(l{=}0, m{=}0, n{=}0|\tau_k, \lambda^T, \lambda^R, \lambda^D) = \begin{cases} 1, & \text{LOS}, k = 1 \\ 0, & \text{LOS}, k > 1 \\ 0, & \text{NLOS} \end{cases}.$$

B. Comparing the three models

The benchmark model cannot account for the average increase in the frequency parameter with the delay of the path observed in the measured sample set in III-A. In consequence, the model parameter α tends to be higher than the sample value for paths arriving earlier in the profile and smaller for paths arriving later in the profile. This justifies the poorest fit of the three models as indicated through the values of e in Table IV. While the GTD-based model does account for the average increase in the frequency parameter with delay and in turn delivers a lower model error than the benchmark, it still assumes frequency-dependence solely on the diffraction mechanism whose component value $\alpha^E = 0.5$ is valid only

TABLE IV

PARAMETER AND ERROR VALUES OF THE THREE FREQUENCY MODELS.

building	GTD-based model		Proposed model				Benchmark model		
	$\lambda^D(\frac{1}{ns})$	$e(\frac{1}{ps})$	$\lambda^T(\frac{1}{ns}), \alpha^T$	$\lambda^R(\frac{1}{ns}), \alpha^R$	$\lambda^D(\frac{1}{ns}), \alpha^D$	$e(\frac{1}{ps})$	α^{LOS}	α^{NLOS}	$e(\frac{1}{ps})$
NIST North	0.037	1.400	0.028, 0.124	0.042, 0.092	0.013, 0.694	0.279	0.052	1.191	3.181
Child Care	0.043	1.924	0.033, 0.215	0.054, 0.069	0.017, 0.536	0.645	0.094	1.965	4.306
Sound	0.031	7.039	0.015, 0.621	0.038, 0.051	0.013, 0.424	2.324	0.022	3.644	17.871

for materials with infinite conductivity. The proposed model relaxes this assumption in featuring parameters to characterize non-metal buildings as well, offering the greatest flexibility to fit the sample set with the least error.

Muqaibel measured the insertion loss and dielectric constant of ten typical wall materials as a function of frequency [25], [26], two of which coincide with the wall materials in *NIST North* and *Sound*. The trend of α-parameters of the proposed model are consistent with their experiments: 1. the logarithmic slope of the insertion loss like to α^T is much smaller for sheet rock than for cinder block; 2. the dielectric constant which characterizes the reflection coefficient is much less frequency-dependent than the insertion loss, also witnessed in our experiments through relatively smaller values of α^R compared to α^T.

VI. CONCLUSIONS

Building on the Geometric Theory of Diffraction, this paper develops a novel model for the frequency-dependence of individual multi-path arrivals in a channel based on the number of transmission, reflections, and diffractions on their paths between the transmitter and receiver. In order to extract the parameters of the model, we conducted a channel measurement campaign consisting of a total of 3000 frequency sweeps from 2-6.5 GHz in three separate buildings combined with raytracing simulations. The proposed model fits the gathered data more closely than existing models, moreover its parameters characterizing the frequency-dependence of the building materials are consistent with values previously recorded for the insertion loss and dielectric constant of those buildings.

REFERENCES

[1] A.F. Molisch, "Ultrawideband Propagation Channels-Theory, Measurement, and Modeling," *IEEE Trans. on Vehicular Technology*, vol. 54, vo. 5, Sept. 2005.

[2] D. Cassioli, M.Z. Win, and A.F. Molisch, "The Ultra-Wide Bandwidth Indoor Channel: From Statistical Model to Simulations," *IEEE Journal on Selected Areas in Communications*, vol. 20, no. 6, Aug. 2002.

[3] Z. Irahhauten, H. Nikookar, and G.J.M. Janssen, "An Overview of Ultra Wide Band Indoor Channel Measurements and Modeling," *IEEE Microwave and Wireless Components Letters*, vol. 14, No. 8, Aug. 2004.

[4] S.M. Yano, "Investigating the Ultra-Wideband Indoor Wireless Channel," *IEEE Conf. on Vehicular Technology, Spring*, May 2002.

[5] C. Prettie, D. Cheung, L. Rusch, and M. Ho, "Spatial Correlation OF UWB Signals in a Home Environment," *IEEE Conf. on Ultra Wideband Systems and Technologies*, May 2002.

[6] A. Durantini, W. Ciccognani, and D. Cassioli, "UWB Propagation Measurements by PN-Sequence Channel Sounding," *IEEE Conf. on Communications*, June 2004.

[7] A. Durantini and D. Cassioli, "A Multi-Wall Path Loss Model for Indoor UWB Propagation," *IEEE Conf. on Vehicular Technology, Spring*, May 2005.

[8] J. Kunisch and J. Pump, "Measurement Results and Modeling Aspects for UWB Radio Channel," *IEEE Conf. on Ultra Wideband Systems and Technologies*, May 2002.

[9] J. Keignart and N. Daniele, "Subnanosecond UWB Channel Sounding in Frequency and Temporal Domain," *IEEE Conf. on Ultra Wideband Systems and Technologies*, May 2002.

[10] S.S. Ghassemzadeh, L.J. Greenstein, T. Sveinsson, A. Kavcic, and V. Tarokh, "UWB Delay Profile Models for Residential and Commercial Indoor Environments," *IEEE Trans. on Vehicular Technology*, vol. 54, no. 4, July 2005.

[11] A.F. Molisch, K. Balakrishnan, D. Cassioli, C.-C. Chong, S. Emami, A. Fort, J. Karedal, J. Kunisch, H. Schantz, U. Schuster, and K. Siwiak, "A Comprehensive Model for Ultrawideband Propagation Channels," *IEEE Conf. on Global Communications*, March 2005.

[12] W. Zhang, T.D. Abhayapala, and J. Zhang, "UWB Spatial-Frequency Channel Characterization," *IEEE Vehicular Technology Conference, Spring*, May 2006.

[13] H. Hashemi, "The Indoor Radio Propagation Channel," *Proceedings of the IEEE*, vol. 81, no. 7, pp. 943-968.

[14] X. Li. and K. Pahlavan, "Super-Resolution TOA Estimation With Diversity for Indoor Geolocation," *IEEE Trans. on Wireless Communications*, vol. 3, no. 1, Jan. 2004.

[15] S. Zwierzchowski and P. Jazayeri, "A Systems and Network Analysis Approach to Antenna Design for UWB Communiations," *IEEE Antennas and Propagation Society Symp.*, June 2003.

[16] A. Moghaddar, Y. Ogawa, and E.K. Wolton, "Estimating the Time-Delay and Frequency Decay Parameter of Scattering Components Using a Modified MUSIC Algorithm," *IEEE Trans. on Antennas and Propagation*, vol. 42, no. 10, Oct. 1994.

[17] R. Carriere and R.L. Moses, "High Resolution Radar Target Modeling Using a Modified Prony Estimator," *IEEE Trans. on Antennas and Propagation*, vol. 40, no. 1, Jan. 1992.

[18] R.C. Qiu and I.-T. Lu, "Multipath Resolving with Frequency Dependence for Wide-Band Wireless Channel Modeling," *IEEE Trans. on Vehicular Technology*, vol. 28, no. 1, Jan. 1999.

[19] L.C. Potter, D.-M. Chiang, R. Carriere, and M.J. Gerry, "A GTD-Based Parametric Model for Radar Scattering," *IEEE Trans. on Antennas and Propagation*, vol. 43, no. 10, Oct. 1995.

[20] A. Papoulis, "Probability, Random Variables, and Stochastic Processes," *McGraw-Hill, Inc.*, Third Edition, 1991.

[21] A. D. Whalen, "Detection of Signals in Noise," *Academic Press, Inc.*, First Edition, 1971.

[22] R. Luebbers, "Finite Conductivity Uniform GTD Versus Knife Edge Diffraction in Prediction of Propagation Path Loss," *IEEE Trans. on Antennas and Propagation*, vol. 32, no. 1, Jan. 1984.

[23] http://cm.bell-labs.com/cm/cs/who/bwk/wise/index.html.

[24] V. Erceg, S. Fortune, J. Ling, A. Rustako, R. Valenzuela, "Comparisons of a Computer-Based Propagation Prediction Tools with Experimental Data Collected in Urban Microcellular Environments," *IEEE Journal on Selected Areas in Communications*, vol. 15, no. 4, May 1997.

[25] A. Muqaibel, S.-J. Bayram, A.M. Attiya, S.M. Riad, "Ultrawideband Through-the-Wall Propagation," *IEE Proceedings on Microwaves, Antennas and Propagation*, vol. 152, no. 6, Dec. 2005.

[26] A. Muqaibel, A. Safaai-Jazi, A. Bayram, and S.M. Riad, "Ultra Wideband Material Characterization for Indoor Propagation," *IEEE Antennas and Propagation Society Sympo.*, June 2003.